Proceedings of the ASME 2018: Turbomachinery Technical Conference and Exposition
GT2018
June 11-15, 2018, Oslo, Norway

GT2018-76811

A NEW MODEL APPROACH FOR CONVECTIVE WALL HEAT LOSSES IN DQMOM-IEM SIMULATIONS FOR TURBULENT REACTIVE FLOWS

Yeshaswini Emmi, Andreas Fiolitakis, Manfred Aigner

German Aerospace Centre (DLR),
Institute of Combustion Technology,
Pfaffenwaldring 38-40, D-70569 Stuttgart, Germany

Franklin Genin, Khawar Syed

GE (Switzerland) GmbH,
Brown Boveri Strasse 7,
5400 Baden, Switzerland

ABSTRACT

A new model approach is presented in this work for including convective wall heat losses in the Direct Quadrature Method of Moments (DQMoM) approach, which is used here to solve the transport equation of the one-point, one-time joint thermochemical probability density function (PDF). This is of particular interest in the context of designing industrial combustors, where wall heat losses play a crucial role. In the present work, the novel method is derived for the first time and validated against experimental data for the thermal entrance region of a pipe. The impact of varying model-specific boundary conditions is analysed. It is then used to simulate the turbulent reacting flow of a confined methane jet flame. The simulations are carried out using the DLR in-house Computational Fluid Dynamics (CFD) code THETA. It is found that the DQMoM approach presented here agrees well with the experimental data and ratifies the use of the new convective wall heat losses model.

INTRODUCTION

Closure of the chemical source term poses one of the greatest challenges in modelling turbulent reactive flows. For this reason, transported probability density function (PDF) methods are an attractive modelling approach for the simulation of turbulent reactive flows, as the chemical source term appears in closed form. The Direct Quadrature Method of Moments (DQMoM) approach for solving the transported PDF equations retains the particular advantage of an already closed chemical source term, while additionally keeping computational costs relatively low compared to the traditional stochastic approaches for solving the PDF transport equation (e.g. Lagrangian Monte-Carlo methods [1] or stochastic field methods [2]). This makes the DQMoM model approach useful most notably for industrial applications, where in particular large domains are required; in addition, larger detailed reaction mechanisms become more accessible due to the lower computational expense offered by DQMoM.

One particular disadvantage of the general transported PDF method is that terms involving diffusive fluxes of heat and mass are unclosed and require modelling. A variety of mixing models are available for these unknown terms, which typically provide a model for scalar dissipation. However, very few models exist which allow the inclusion of convective wall heat losses [3–5]. None of these models have been used to the authors' knowledge in the DQMoM approach for solving the PDF transport equation. The implementation of convective wall heat losses is especially relevant in the context of industrial combustors, where for example engine cooling capabilities can play a major role in combustor design. Wall heat losses can also significantly influence the combustion process itself, and accurate prediction of this phenomenon is crucial in forecasting, for instance, cooling efficiency and its impact on noxious emissions and dynamics.

Although current literature provides some insight into the capabilities of the DQMoM model in turbulent reactive flow regimes [6–10], there is little in the way of (a) wall heat losses and (b) quantification of the influence of boundary conditions. In the present work, a method for including convective wall heat

losses at isothermal walls in the DQMoM method is therefore derived for the first time; the required inclusion of molecular diffusion in the governing equations is demonstrated. This method is first validated against experimental data of a thermal entrance region of a pipe using data provided by Abbrecht and Churchill [11]. The impact of varying model-specific boundary conditions for this case is also analysed. Next, the model is verified for turbulent reacting flows with the use of a confined methane jet flame against data obtained from experiments carried out by Lammel et al. [12]. The steady Reynolds-Averaged Navier-Stokes (RANS) approach is used for all presented cases, and detailed chemical kinetics are used to model chemistry. The simulations are carried out using the in-house Computational Fluid Dynamics (CFD) code THETA [13, 14] of the German Aerospace Centre (DLR).

THEORY

DQMoM is an alternative approach to the traditional stochastic methods of solving the transport equations of thermochemical PDFs [15]. In this work, a joint PDF of specific enthalpy and linearly independent species mass fractions is used. For low Mach number flows the assumption of constant thermodynamic pressure is valid, and these variables are sufficient to completely determine the thermodynamic state of the chemically reacting flow. The following section first presents the Favre-PDF equation and the models used to handle unclosed terms, then the DQMoM-IEM equations used to solve the Favre-PDF equation, and finally the convective wall heat losses model for the DQMoM-IEM approach.

Favre-PDF Equation

The Favre-PDF $\widetilde{P}$ is defined as:

$$\widetilde{P}(\psi_\alpha;x_i,t) = \frac{\rho(\psi_\alpha)P(\psi_\alpha;x_i,t)}{\langle\rho\rangle(x_i,t)} \tag{1}$$

where ρ is the density, ψ_α the state vector corresponding to ϕ_α, which is the vector of the thermochemical variables specific enthalpy, h, and species mass fraction, Y_α (which are both random variables in a turbulent flow). P is the thermochemical PDF and x_i and t are the space and time coordinates respectively. The qualifier $\widetilde{(\cdot)}$ represents a Favre-averaged quantity and $\langle\cdot\rangle$ a Reynolds-averaged quantity. For the DQMoM apporach, this Favre-PDF is approximated by a finite number of Dirac pulses δ as:

$$\widetilde{P}(\psi_\alpha;x_i,t) = \sum_{n=1}^{N_e} p_n(x_i,t) \prod_{\alpha=1}^{N_s} \delta(\psi_\alpha - \langle\phi_\alpha\rangle_n(x_i,t)) \tag{2}$$

where N_e is the number of environments and N_s is the number of scalars in the vector ϕ_α. The probability of each environment is denoted as p_n and satisfies the condition $\sum_{n=1}^{N_e} p_n = 1$. Assuming now that differential diffusion is negligible and Lewis number $Le = 1$, the unclosed form of the Favre-PDF transport equation reads (using Einstein notation, as with the rest of the paper) [16]:

$$\begin{aligned}\frac{\partial(\langle\rho\rangle\widetilde{P})}{\partial t} + \frac{\partial(\langle u_i|\phi_\gamma=\psi_\gamma\rangle\langle\rho\rangle\widetilde{P})}{\partial x_i} \\ = -\frac{\partial}{\partial\psi_\alpha}\left(\frac{\partial}{\partial x_i}\left\langle D\frac{\partial\phi_\alpha}{\partial x_i}\middle|\phi_\gamma=\psi_\gamma\right\rangle\langle\rho\rangle\widetilde{P}\right) \\ -\frac{\partial}{\partial\psi_\alpha}\left(\langle S_\alpha|\phi_\gamma=\psi_\gamma\rangle\frac{\langle\rho\rangle}{\rho}\widetilde{P}\right)\end{aligned} \tag{3}$$

where $\langle\cdot|\phi_\gamma=\psi_\gamma\rangle$ denotes a conditional expectation for given ψ_γ. The velocity is expressed by u_i, the molecular diffusion coefficient by D and the chemical source term is S_α. The second term on the left hand side (LHS) of Eq. (3) and the first term on the right hand side (RHS) are unclosed terms, and require closure models.

Closure Models The first unclosed term in Eq. (3) is treated using the Gradient Diffusion Model (GDM) [1, 17]:

$$\begin{aligned}\frac{\partial(\langle u_i|\phi_\gamma=\psi_\gamma\rangle\langle\rho\rangle\widetilde{P})}{\partial x_i} &= \frac{\partial}{\partial x_i}\left(\langle u_i|\phi_\gamma=\psi_\gamma\rangle\langle\rho\rangle\widetilde{P}\right) \\ &= \frac{\partial}{\partial x_i}\left(\langle\widetilde{u}_i|\phi_\gamma=\psi_\gamma\rangle\langle\rho\rangle\widetilde{P}\right) \\ &\quad + \frac{\partial}{\partial x_i}\left(\langle u_i''|\phi_\gamma=\psi_\gamma\rangle\langle\rho\rangle\widetilde{P}\right) \\ &= \frac{\partial(\widetilde{u}_i\langle\rho\rangle\widetilde{P})}{\partial x_i} - \frac{\partial}{\partial x_i}\left(\langle\rho\rangle D_T\frac{\partial\widetilde{P}}{\partial x_i}\right)\end{aligned} \tag{4}$$

where $(\cdot)''$ is a quantity representing fluctuation over Favre-average. The term D_T is the turbulent diffusion coefficient. The second unclosed term in Eq. (3) is algebraically manipulated to result in the following [18]:

$$-\frac{\partial}{\partial\psi_\alpha}\left(\frac{\partial}{\partial x_i}\left\langle D\frac{\partial\phi_\alpha}{\partial x_i}\middle|\phi_\gamma=\psi_\gamma\right\rangle\langle\rho\rangle\widetilde{P}\right)$$
$$=\frac{\partial}{\partial x_i}\left(\langle\rho\rangle D\frac{\partial\widetilde{P}}{\partial x_i}\right)+\frac{\partial}{\partial x_i}\left(D\widetilde{P}\frac{\partial\langle\rho\rangle}{\partial x_i}\right) \tag{5}$$
$$-\langle\rho\rangle\frac{\partial^2}{\partial\psi_\alpha\partial\psi_\beta}\left(\left\langle D\frac{\partial\phi_\alpha}{\partial x_i}\frac{\partial\phi_\beta}{\partial x_i}\middle|\phi_\gamma=\psi_\gamma\right\rangle\widetilde{P}\right)$$

The second term on the RHS of Eq. (5), spatial density gradients, can be altogether neglected [18]. The third term represents scalar dissipation, and is closed using the Interaction by Exchange with the Mean (IEM) model [19].

Molecular Diffusion The first term on the RHS of Eq. (5) represents the molecular diffusion. This term is essential when considering convective wall heat losses as molecular diffusion plays an important role in transferring heat from the wall to the fluid, and thus needs to be included in the transport equation. It is observed that this term has the same form as the GDM term in Eq. (4). The two can therefore be combined:

$$\frac{\partial}{\partial x_i}\left(\langle\rho\rangle D_T\frac{\partial\widetilde{P}}{\partial x_i}\right)+\frac{\partial}{\partial x_i}\left(\langle\rho\rangle D\frac{\partial\widetilde{P}}{\partial x_i}\right)$$
$$=\frac{\partial}{\partial x_i}\left(\langle\rho\rangle D_{eff}\frac{\partial\widetilde{P}}{\partial x_i}\right) \tag{6}$$

providing an effective diffusivitiy $D_{eff}=D_T+D$. For cases where molecular diffusion does not play a pivotal role, D can simply neglected, establishing a simple on-off function for molecular diffusivity.

Thus, re-writing Eq. (3) using the closure models elaborated above and the molecular diffusion term, the final form of the transport equation for the joint thermochemical Favre-PDF of specific enthalpy and species mass fractions $\widetilde{P}$ is [16]:

$$\frac{\partial(\langle\rho\rangle\widetilde{P})}{\partial t}+\frac{\partial(\widetilde{u}_i\langle\rho\rangle\widetilde{P})}{\partial x_i}-\frac{\partial}{\partial x_i}\left(\langle\rho\rangle D_X\frac{\partial\widetilde{P}}{\partial x_i}\right)$$
$$=-\frac{\partial}{\partial\psi_\alpha}\left(\left(\frac{C_\phi}{2\tau_t}(\widetilde{\phi}_\alpha-\psi_\alpha)+\frac{S_\alpha}{\rho}\right)\langle\rho\rangle\widetilde{P}\right) \tag{7}$$

where D_X is either the turbulent diffusion coefficient D_T (when molecular diffusion is neglected) or effective diffusion coefficient D_{eff} (when molecular diffusion is accounted for), $C_\phi=2.0$ is the IEM mixing model constant and τ_t is the integral turbulent time scale.

DQMoM-IEM Approach

The DQMoM-IEM model approach is now used to solve Eq. (7). The method essentially involves forcing the definition of the Favre-PDF $\widetilde{P}$, i.e. Eq. (1), to agree with values of the known (or calculable) statistical moments such that [15]:

$$\langle\phi_1^{m_1}\cdots\phi_{N_s}^{m_{N_s}}\rangle=\sum_{n=1}^{N_e}p_n\prod_{\alpha=1}^{N_s}\langle\phi_\alpha\rangle_n^{m_\alpha} \tag{8}$$

This results in a set of transport equations for p_n and $\langle\phi_\alpha\rangle_n$. For $N_e=2$ (generally sufficient[1]), we obtain a total of $1+2N_s$ equations:

$$\frac{\partial(\langle\rho\rangle p_n)}{\partial t}+\frac{\partial(\widetilde{u}_i\langle\rho\rangle p_n)}{\partial x_i}-\frac{\partial}{\partial x_i}\left(\langle\rho\rangle D_X\frac{\partial p_n}{\partial x_i}\right)=a_n \tag{9}$$

$$\frac{\partial(\langle\rho\rangle\langle s_\alpha\rangle_n)}{\partial t}+\frac{\partial(\widetilde{u}_i\langle\rho\rangle\langle s_\alpha\rangle_n)}{\partial x_i}-\frac{\partial}{\partial x_i}\left(\langle\rho\rangle D_X\frac{\partial\langle s_\alpha\rangle_n}{\partial x_i}\right)=b_{\langle\phi_\alpha\rangle n} \tag{10}$$

where $\langle s_\alpha\rangle_n=p_n\langle\phi_\alpha\rangle_n$ are the probability-weighted scalars. These are the final transport equations used in the DQMoM-IEM approach. The RHS of Eq. (9), a_n, is set to zero: this keeps the number of necessary transport equations to $(N_e-1)+N_sN_e$, and ensures that the boundedness of the conditional means is not violated [15]. The source term $b_{\langle\phi_\alpha\rangle n}$ on the RHS of Eq. (10) is [21]:

$$b_{\langle\phi_\alpha\rangle n}=(-1)^n\langle\rho\rangle\frac{p_1D_X\sum_{i=1}^3\left(\frac{\partial\langle\phi_\alpha\rangle_1}{\partial x_i}\right)^2+p_2D_X\sum_{i=1}^3\left(\frac{\partial\langle\phi_\alpha\rangle_2}{\partial x_i}\right)^2}{\langle\phi_\alpha\rangle_2-\langle\phi_\alpha\rangle_1}$$
$$+\langle\rho\rangle p_n\frac{C_\phi}{2\tau_t}(\widetilde{\phi}_\alpha-\langle\phi_\alpha\rangle_n)+p_n\frac{\langle\rho\rangle S_\alpha}{\rho} \tag{11}$$

The first term in Eq. (11) ensures correct variance. In handling this term when $\langle\phi_\alpha\rangle_2=\langle\phi_\alpha\rangle_1$, the method adopted by Akroyd

[1] In general, 2-environment models have been shown to perform accurately, with no significant improvements in 3- or 4- environment formulations [20]. In this work, mean and variance are the two captured moments.

et al. [10] is implemented in this work. In short, a bounding function and a filter function are used to constrain the variance production term and smooth out singularities/discontinuities respectively.

Convective Wall Heat Losses Model

The aim is to be able to specify boundary conditions for solving the equation for probability-weighted specific enthalpy, Eq. (10), when wall temperature is a given. If a certain temperature $\widetilde{T}_w$ is required to be set on an isothermal wall, it follows that this $\widetilde{T}_w$ can no longer be considered a random variable as it is a known quantity. In terms of the marginal PDF of temperature, this means that it relaxes asymptotically from the two distinct Dirac pulses in Eq. (2) into a single Dirac pulse as the isothermal wall is approached. For DQMoM, this implies that both environments $\langle T_w \rangle_1$ and $\langle T_w \rangle_2$ have the same value. This wall temperature is thus used in conjunction with the composition on the wall in order to calculate the enthalpy for each environment, which are used as boundary conditions for solving Eq. (10).

For the present implementation that uses bounding and filter functions, identical environmental values result in the first term of Eq. (11) being set to zero, which leads to the variances of enthalpy (and therefore temperature) being reproduced incorrectly. In order to circumvent this situation, $\langle T_w \rangle_1$ and $\langle T_w \rangle_2$ are set to be unique by perturbing the prescribed wall temperature $\widetilde{T}_w$ by a small, arbitrarily chosen $\pm\varepsilon$:

$$\langle T_w \rangle_n = \widetilde{T}_w + (-1)^n \frac{\varepsilon}{p_{w,n}} \tag{12}$$

This method ensures that (a) the mean, i.e. the prescribed wall temperature, is preserved and that (b) the variances of temperature and specific enthalpy are accurately reproduced. Additionally, molecular diffusion is accounted for using Eq. (6), and $D_X = D_{eff} = D_T + D$ is used.

Turbulence model

The standard k-ω turbulence model [22] is used for both studied test cases, with an incompressible solver for the momentum equations. Pressure is solved using the steady-state Semi-Implicit Method for Pressure Linked Equations (SIMPLE) [23]. The models are implemented in the DLR in-house code THETA, which is based on a finite volume discretisation method. The transport processes and chemistry are solved in a coupled fashion. THETA allows also for the inclusion of detailed reaction mechanisms.

TEST CASES

The present work considers two different test cases. Both are used to validate and verify the implementation of the wall heat losses model within DQMoM in the DLR in-house code THETA. The first test case considers experiments conducted on the thermal entrance region of a mixing pipe by Abbrecht and Churchill [11]. This experiment provides a simple set-up, ideal for the initial validation of the model presented in this paper for an inert flow. Furthermore, the influence of varying model-specific boundary conditions is quantified. The second test case investigates a confined methane jet flame and uses data gathered by Lammel et al. [12], serving to validate the use of the new model with the inclusion of combustion kinetics in a lab-scale burner. Both test cases provide measurement uncertainty data.

Thermal Entrance Region of a Pipe

Experiments conducted by Abbrecht and Churchill [11] are used in this work to validate DQMoM for convective wall heat losses for a non-reacting case. A long mixing pipe of diameter $d_{mp} = 3.861 \times 10^{-2}$ m with a step increase in wall temperature was used, with a turbulent, fully developed flow of air. Measurements were conducted for flow Reynolds numbers of approximately $Re = 15{,}000$ and $65{,}000$ with corresponding flow rates of approximately $\dot{m} = 8.391 \times 10^{-3}$ kg/s and 3.654×10^{-2} kg/s. The unheated length of the tube was 1.676 m, and a variable-length wall-heated section followed, ending in an additional unheated tube opening out into atmosphere. The length of the heated tube was manipulated to allow the heating distance to the centre of the fixed calorimeter to vary from $0.453 d_{mp}$ to $9.97 d_{mp}$. The inlet temperatures were at $T_{in} = 299.46$ K and then at 300.81 K for the higher Re run, with the corresponding heated wall temperatures of $T_w = 313.21$ K and 315.09 K. Plastic discs were used as insulation for the non-heated sections. Hot-wire anemometry was used to measure velocity and temperature profiles, with a probe located downstream of the calorimeter.

Confined Jet Flame

In order to validate the use of the DQMoM wall heat loss implementation in reacting flow, a confined atmospheric methane jet flame experiment conducted by Lammel et al. [12] is used in this work. The experimental set-up consisted of a tube of diameter $d_{cjf} = 10$ mm leading into a rectangular cross-sectioned combustion chamber of dimensions $5d_{cjf} \times 4d_{cjf}$ with height $60d_{cjf}$. The inlet pipe was set off-centre to ensure a one-sided recirculation zone; it also rose into the combustion chamber by $2d_{cjf}$. A schematic of the set-up is shown in Fig. 1. Statically premixed methane/air was fed into the inlet nozzle at atmospheric pressure with speed varying from 90 to 150 m/s, and corresponding Reynolds numbers ranging from $Re = 13{,}983$ to $42{,}410$. The mixture was preheated to 473 K, 573 K and 673 K. The mixture composition was varied by starting at stoichiometric condi-

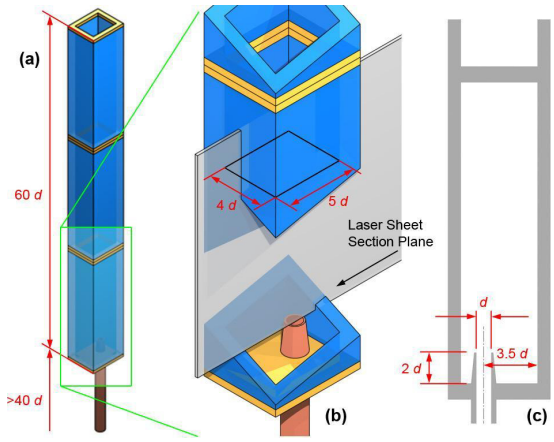

FIGURE 1. EXPERIMENTAL SET-UP OF THE CONFINED JET FLAME [12].

tions and then being decreased until the flame showed signs of instability or lean blow out. OH-PLIF and OH*-CL were carried out in order to enable visualisation of the flame position, shape and stabilisation. Raman data were also extracted, such that major species concentrations, mixture fraction and temperature could be determined. Fig. 1(b) shows the laser sheet plane upon which these measurements were carried out. Furthermore, PIV was used to obtain planar velocity fields at various section planes.

Numerical Set-Up

Structured hexahedral meshes are used for both the pipe and the confined jet flame cases. For the former, the computational grid is reduced to that of a wedge, making use of the rotational symmetry present in the experimental setup; it consists of approximately 20,000 nodes. The y^+ at the wall is approximately 1.5, and no wall functions are used with the $k-\omega$ turbulence model. The inflow conditions for this test case are shown in Tab. 1. In order to observe the influence of the different boundary conditions, the inlet environment probabilities were varied from $p_1 = 0.1$ to 0.4 in 0.1 increments, in addition to a mass-fraction scaled value of 0.233. Furthermore, the value of ε from Eq. (12) was also varied from $\varepsilon = 1\times10^{-5}$ K to 1×10^{-1} K in steps of 1×10^{-1}, with p_1 constant at 0.233 across the ε range. The inlet compositions and temperatures in each environment were kept identical to one another at the mean physical values.

The confined jet flame grid uses the symmetry present in the set-up and consists of half the combustion chamber and nozzle, split down the section plane seen in Fig. 1(b); it comprises approximately 2.5M nodes. The boundary conditions used for this work are summarised in Tab. 2. The value for probability of environment 1 at the inlet was scaled to the mass fraction of the fuel, $p_1 = Y_{CH_4} = 0.0398$. The inlet temperatures and species mass

TABLE 1. Boundary Conditions for the Mixing Pipe.

		Inlet	Wall
Velocity	[m/s]	6.287	0.0
Species	[-]	O_2, N_2	-
Mass Fractions	[-]	0.233, 0.767	-
Temperature	[K]	301.03	313.52
p_1	[-]	0.233	-

TABLE 2. Boundary Conditions for the Confined Jet Flame.

		Inlet	Isothermal Walls
Velocity	[m/s]	150	0.0
Species	[-]	CH_4, O_2, N_2	-
Mass Fractions	[-]	0.0398, 0.2236, 0.7365	-
Temperature	[K]	573	800
p_1	[-]	0.0398	-

fractions for both environments were treated differently to the inert test case. In order to provoke non-zero variance for these quantities (since, in contrast to the inert case, species variance should be non-zero due to combustion), the two environments were perturbed slightly away from one another about the mean physical value, similar to Eq. (12):

$$\langle Y_{\alpha,in}\rangle_n = \widetilde{Y}_{\alpha,in} + (-1)^n \frac{1\times10^{-5}}{p_{in,n}} \tag{13}$$

where $(\cdot)_{in}$ denotes an inlet quantity. The walls of the inflow nozzle were set to be adiabatic, and the walls of the combustion chamber were prescribed as isothermal at 800 K. The value for ε in Eq. (12) was kept constant at 1×10^{-5} K. For modelling the chemistry, a detailed methane oxidation reaction mechanism [24] with 19 reacting and 2 non-reacting species and 84 reactions was used. For this simulation, the effect of gravity was also taken into account.

It is important to note that each of the two test cases considered in this work have only one inflow boundary, which means that the prescription of DQMoM boundary conditions is not trivial. The issue can be summarised as follows. Previous works utilising the DQMoM model have always had two or more inflow

boundaries, allowing for physically meaningful designations for the environmental values of species and temperature either (a) through control of p_n: each environment can be turned "on" or "off" ($p_1 = 1$, $p_2 = 0$ and vice-versa) at the inlet depending on the specific combination of species and temperature required at that inlet (the two environments are different to one another but do not vary from inlet to inlet); or (b) allowing for the whole spectrum of p_n by having the two environments identical to one another at each inlet, but varying from inlet to inlet. Since for premixed flows only option (b) is sensible, i.e. both environments are identical to each other and p_n can theoretically be assigned arbitrarily, the authors consider that the most reasonable approach is to scale the inlet probabilities to the species mass fractions (of fuel/oxidiser when relevant). This emulates an artificially non-premixed system, i.e. $p_1 = Y_{i,1}$ would be the result of prior mixing. As outlined above, the effect of varying $p_{in,n}$ is investigated in the first test case.

This approach is naturally not viable if the number of environments were to be increased. Previous works using e.g. three environments have used again either option (a) or (b) mentioned above. The premixed case requires special consideration. The only reasonable approach for premixed cases using more than two environments might be to split the probabilities arbitrarily across the number of environments, with the species and temperature values slightly perturbed about the mean (as it is now). This is not entirely clear yet, and for such cases, further investigation is necessary.

RESULTS

Pipe Thermal Entrance Region

The simulation results obtained for the mixing pipe are presented here. Figure 2 compares the experimental data of the temperature distribution with the results from DQMoM-IEM for various positions downstream of the inlet. The x-axis of the graph is the normalised distance from the centre of the pipe to the wall, with the y-axis showing a normalised temperature of the form $\frac{\widetilde{T}-\widetilde{T}_{in}}{\widetilde{T}_w-\widetilde{T}_{in}}$ with $\widetilde{T}_{in}$ being the inlet temperature and $\widetilde{T}_w$ the wall temperature. The simulation results in this graph are for mass fraction-scaled $p_1 = 0.233$ and $\varepsilon = 1 \times 10^{-5}$ K. The experiment reports various uncertainty data; for the temperature measurements, ± 0.11 K is estimated.

The results obtained from the simulation agree very well with the experimental data. The largest deviations are found at a downstream location of $x/d_{mp} = 4.12$, but are nevertheless small. The simulation seems to produce a faster transition from the mean flow temperature to the wall temperature, i.e. a higher transfer of heat down from the wall. This is most likely due to over-predicted levels of turbulence in the pipe flow. Figure 3 shows the Favre-RMS (root mean square) data for temperature obtained from simulation. Here, five different runs are considered, with ε ranging from 1×10^{-5} K to 1×10^{-1} K in steps of 1×10^{-1}, and $p_1 = 0.233$ across all five cases.

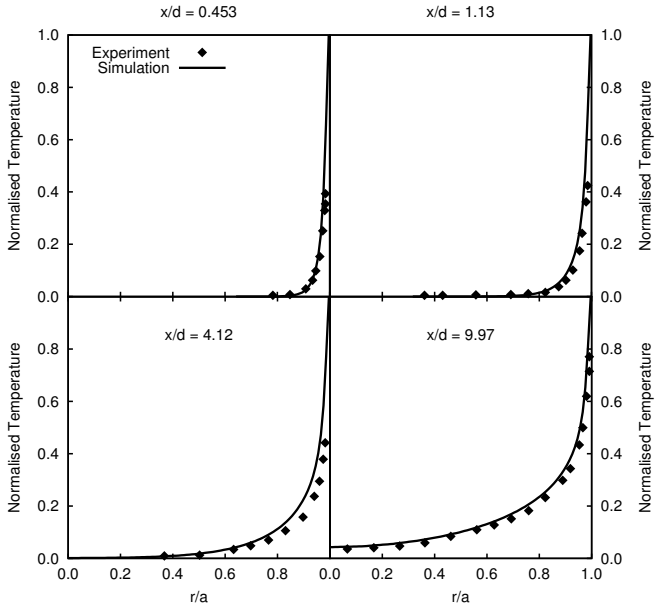

FIGURE 2. TEMPERATURE DISTRIBUTION FOR $p_1 = 0.233$ AND $\varepsilon = 10^{-5}$.

Away from the wall, the RMS does not vary from one simulation to the next; however, some variance is produced at the wall itself (due to the difference in values of $T_{w,1}$ and $T_{w,2}$). As expected, this dwindles to zero as $\varepsilon \to 0$ (this is clear in Fig. 4: smaller perturbations from the mean correspond, naturally, to a lower RMS). Most importantly, the RMS is clearly non-zero in the shear layer for all five cases as required.

Next, the effects of varying the inlet environmental probability is investigated. Figure 5 shows variation of Favre-RMS temperature against normalised radial coordinate, for fixed value of $\varepsilon = 1 \times 10^{-5}$ K and p_1 ranging from 0.1 to 0.4 in steps of 0.1, as well as the mass fraction scaled value of $p_1 = 0.233$. It is clear in Fig. 5 that varying the value of p_1 does not have a notable impact on the RMS of temperature. The most significant variation is visible about halfway between the wall and the centre of the pipe, at the most downstream position of $x/d = 9.97$; the differences cease to manifest as one approaches the wall and further upstream in the flow. At $x/d = 9.97$, the RMS from the $p_1 = 0.1$ simulation lies slighly higher than the rest of the results, and the $p_1 = 0.4$ simulation slightly lower. The mean temperature does not vary across the p_1 spectrum. Without further detailed study, it is difficult to pinpoint the exact source of these discrepancies. They are, however, insignificant enough to justify the assumption that RMS is independent of the choice of inlet p_n. The disparities gradually weaken to non-existence as the peak RMS is approached in the shear layer: the RMS produced due to the steeper temperature gradients in the proximity of the wall begins to take

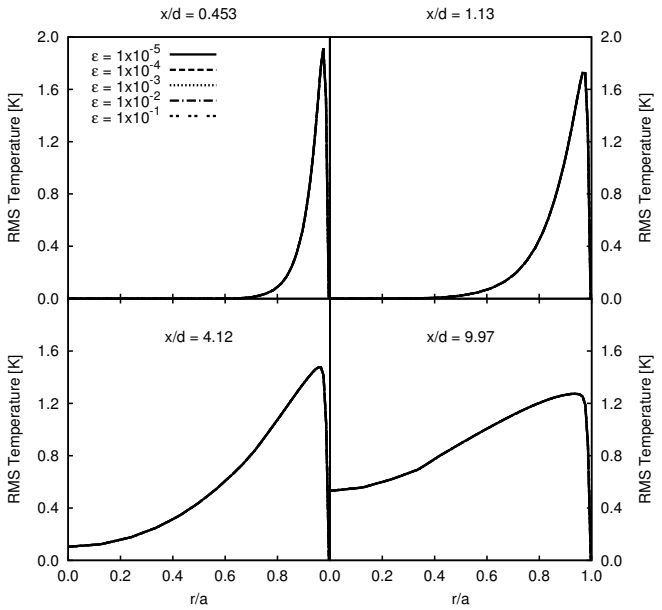

FIGURE 3. FAVRE-RMS OF TEMPERATURE WITH VARYING ε AND $p_1 = 0.233$.

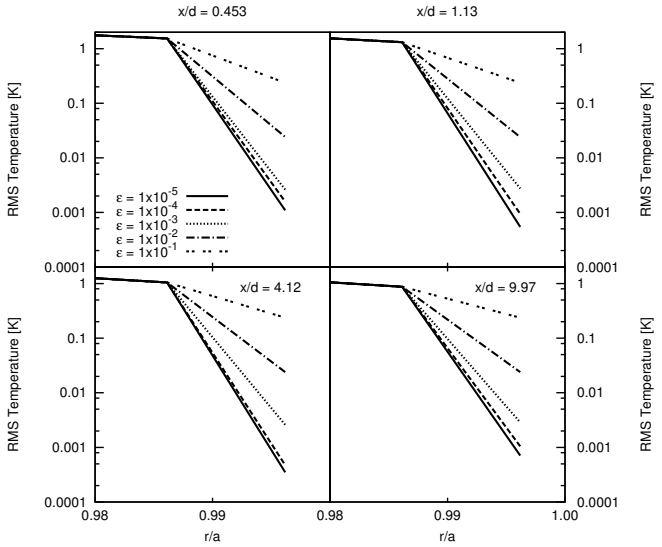

FIGURE 4. FAVRE-RMS OF TEMPERATURE WITH VARYING ε AND $p_1 = 0.233$. SCALE ZOOMED IN TO WALL.

over and eventually dominates completely, i.e. $\langle T \rangle_1$ and $\langle T \rangle_2$ move away from one another independent of the choice of p_1. Further upstream, both environmental temperatures are equal at the central axis (as prescribed at the inlet boundary).

Parameter choices With varying p_1, no variation in the first moment of temperature is observed, and only minimal variation in the second moment. For the next test case, thus, the choice of scaling inlet p_1 to inlet mass fractions (already discussed in the previous section) remains valid. As for choosing the value of the ε perturbation, once again the first moment remains unaffected, and the RMS is identical for all chosen ε away from very close to the wall. It is physically meaningful for temperature RMS exactly at the isothermal wall to be zero. Since $\varepsilon = 1 \times 10^{-5}$ gives the RMS value closest to zero, this is also chosen for the confined jet flame.

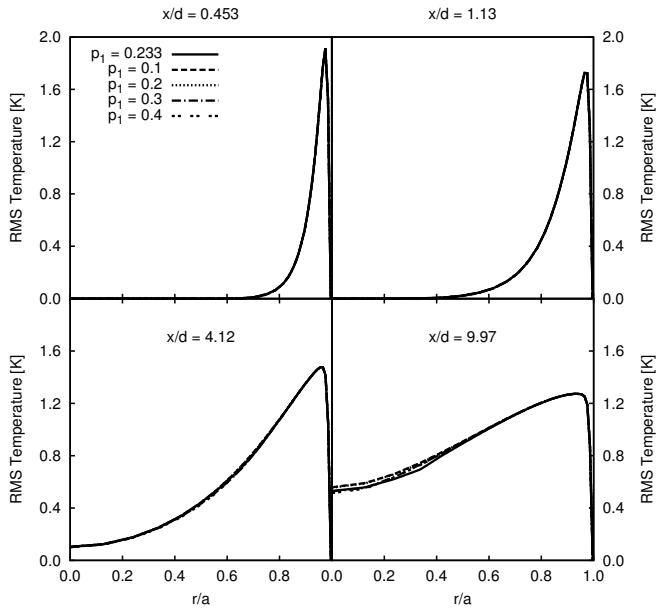

FIGURE 5. FAVRE-RMS OF TEMPERATURE WITH VARYING p_1 AND $\varepsilon = 1 \times 10^{-5}$.

Confined Jet Flame

Data obtained from the DQMoM simulations of the confined jet flame are presented in this section. The flow field and flame region can be visualised by the streamlines of Favre-averaged velocity coloured by axial velocity in Fig. 6 and Favre-averaged temperature in Fig. 7.

A qualitative comparison of the flow field to the experimental data in Fig. 6 shows that the DQMoM-IEM model is able to capture the approximate flow structures very well. The large recirculation zone that stabilises the flame is reproduced qualitatively correctly, though it is shifted further upstream than in the experiment. The temperature contours in Fig. 7 show the approximate shape and position of the jet flame. Hot gas can clearly be seen to have recirculated down from the main flame region to near the nozzle exit. The small section missing from the figure from experiment is due to restrictions faced while conducting the Laser Raman Spectroscopy [12]. The adiabatic flame temperature of 2064 K is higher than the maximum temperature seen in

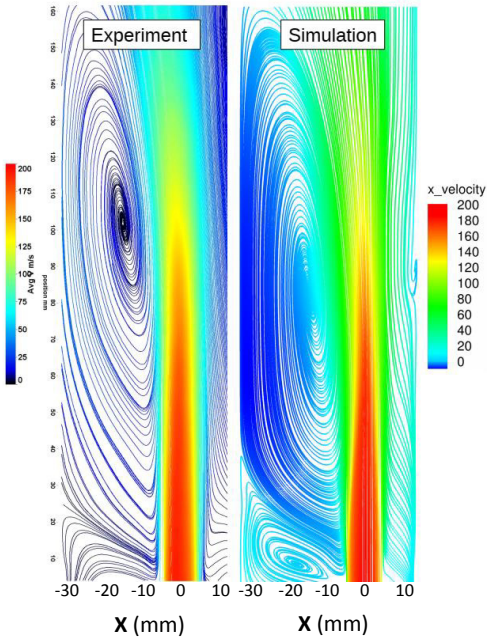

FIGURE 6. AXIAL VELOCITY STREAMLINES [m/s].

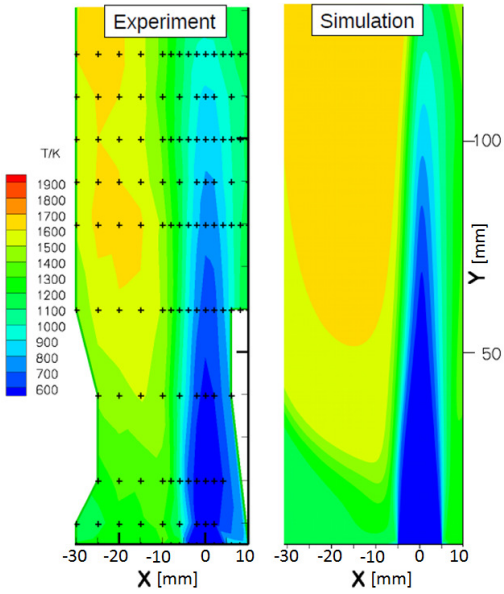

FIGURE 7. FAVRE-AVERAGE OF TEMPERATURE [K].

the experiment/simulation, which highlights the crucial importance of the inclusion of wall heat losses.

A closer look at velocity and temperature profiles, in addition to important species profiles, is shown in Figs. 8 to 11; each shows the relevant quantity against radial coordinate for four different positions downstream of the nozzle.

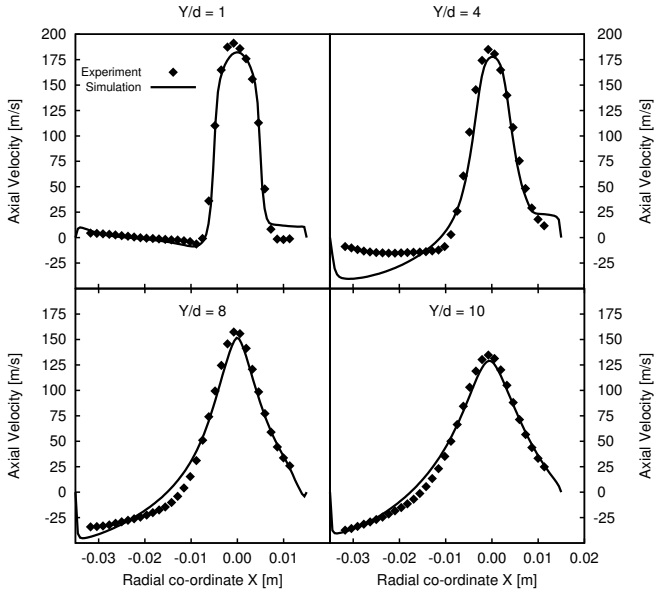

FIGURE 8. FAVRE-AVERAGE OF AXIAL VELOCITY.

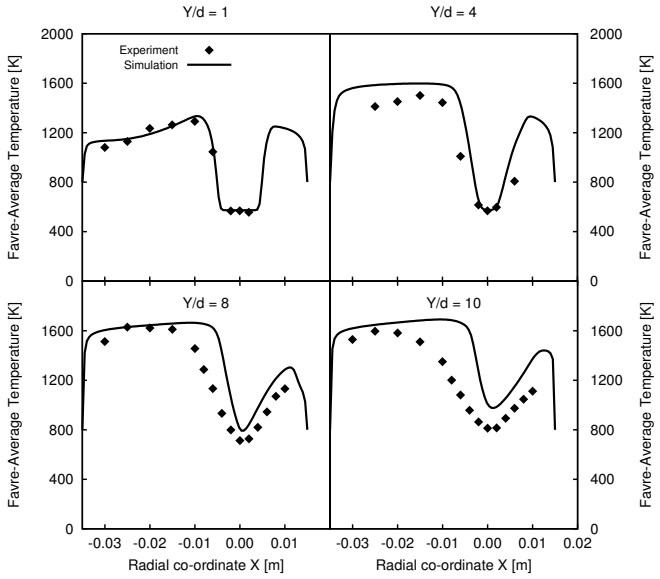

FIGURE 9. FAVRE-AVERAGE OF TEMPERATURE.

Figure 8 plots axial velocity. The overall agreement is very good; however, a few minor deviations are evident. The peak velocities on the nozzle axis are slightly under-predicted by DQMoM and the position of the recirculation zone sits slightly further upstream compared to experiment. The peak velocities in the recirculation zone, on the other hand, are higher in the simulation (i.e. higher positive velocities and lower negative velocities). This may be due to the chosen turbulence model.

The Favre-average of temperature is compared in Fig. 9. The

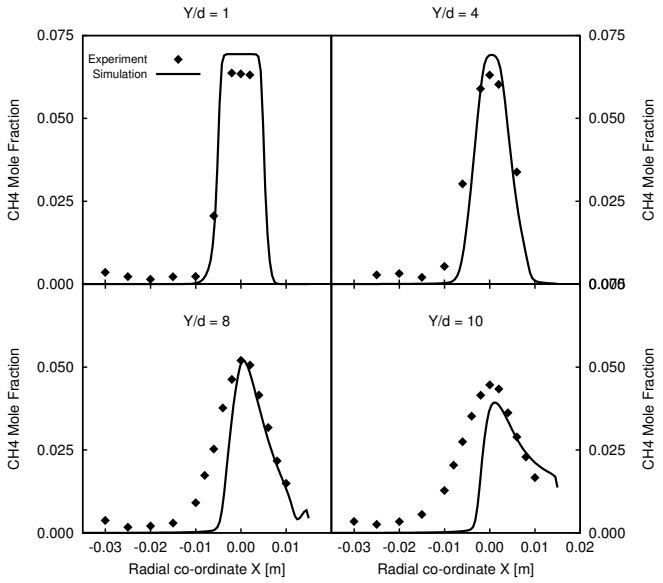

FIGURE 10. FAVRE-AVERAGE OF CH4 MOLE FRACTION.

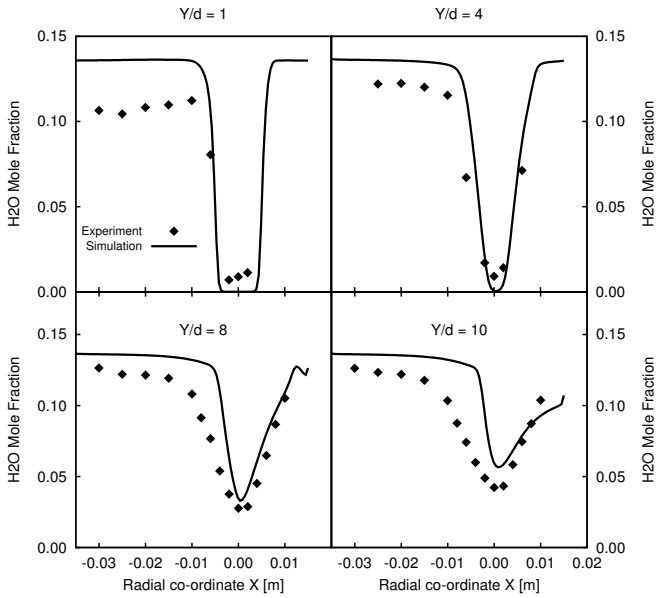

FIGURE 11. FAVRE-AVERAGE OF H2O MOLE FRACTION.

model and experiment agree very well at the most upstream position $Y/d = 1$. The peak flame temperature given by the DQMoM model is higher than that in experiment by around 50 K, which may be a consequence of the chosen reaction mechanism. The high temperatures also plateau across a longer space, whereas the experiment shows a quicker drop in temperature away from the peak. This could indicate the presence of a wider reaction zone in the simulation. The stronger recirculation zone in the simulation might also explain the longer temperature plateau, as hot gases are pushed back upstream more forcefully and amass to a higher degree in this region.

The methane mole fraction plots are in good agreement at the two upstream locations, as Fig. 10 shows. It should be noted that the discrepancy between experiment and simulation in the nozzle region of the flow, for $Y/d = 1$, is due to measurement error (the same region in Fig. 11 also shows minor water presence). Further downstream and on the recirculation zone side of the combustion chamber, the levels of methane in the simulation are much lower than what is seen in the experiment. This is consistent with the picture painted by the temperature plots: the higher and longer-sustained temperatures lead to a higher consumption of fuel. The trend seen in the experiment is recovered further away from the recirculation zone. In the same way, water mole fraction is then higher than predicted in experiment in the same regions, and closer to the experimental data nearer the nozzle axis (see Fig. 11). It is also higher generally in the regions $X < 0$ m, even in the regions where temperature is correctly reproduced; this could be because, as indicated with the temperature plots, the higher water levels produced are transported and collected further upstream due to the stronger recirculation.

Wall Temperature Sensitivity Measurements indicate that the wall temperatures range from approximately 550 K near the nozzle exit to above 1200 K further downstream [25]. A brief sensitivity analysis for wall temperatures was carried out by Gövert et al. [26]: these results seem to suggest minimal influence of the wall temperature on the fluid temperatures and flame structure, making the current choice of a constant 800 K a reasonable one for initial model validation purposes. Although more accurate representation of the wall temperature profile in simulation would likely mean that higher temperatures are observed in the recirculation zone, the overall influence is expected to be small. The nature and position of the recirculation zone, as well as the temperatures predicted by the reaction mechanism, are expected to play a greater role in the combustion behaviour for this particular burner. Nonetheless, in order to confidently quantify the relationship between wall temperature and combustion behaviour, further detailed investigation is necessary.

CONCLUSIONS

The use of the new convective wall heat losses model for isothermal walls in conjunction with the inclusion of molecular diffusion for the DQMoM-IEM model approach shown in this paper has been validated. Two different test cases were studied. The first test case, a non-reacting thermal entrance region of a pipe, was used to validate the implementation of the newly formulated convective wall heat loss model with the inclusion of molecular diffusion. The results of the simulations were found to agree well with the experimental data. The influence of varying boundary conditions for this test case was also carried out;

this particular formulation of the DQMoM model boundary conditions was further demonstrated to be valid for premixed (i.e. single inlet) flows. The new wall heat losses model was then validated for a turbulent reacting flow, using a confined methane jet flame. The importance of accurate reproduction of the recirculation zone was shown, since this had a notable impact on the distribution of temperature and species across the domain. In addition, it was found that the lowering of the peak flame temperatures would have closed the gap between the experimental and simulation results. Overall, however, the results and trends agreed well with the data from experiment; the use of this model for inert and well as reacting flows has been successfully verified.

REFERENCES

[1] Pope, S., 1985. "PDF methods for turbulent reactive flows". *Progress in Energy and Combustion Science,* ***11***, pp. 119–192.

[2] Valiño, L., 1998. "A field monte carlo formulation for calculating the probability density function of a single scalar in a turbulent flow". *Flow, Turbulence and Combustion,* ***60***, pp. 157–172.

[3] Pozorski, J., and Minier, J.-P., 2006. "Stochastic modelling of conjugate heat transfer in near-wall turbulence". *International Journal of Heat and Fluid Flow,* ***27***(5), pp. 867 – 877.

[4] Gerlinger, P., 2017. "Lagrangian transported MDF methods for compressible high speed flows". *Journal of Computational Physics,* ***339***, pp. 68 – 95.

[5] Fiolitakis, A., Ess, P. R., Gerlinger, P., and Aigner, M., 2014. "Modeling of heat transfer and differential diffustion in transported PDF". *Combustion and Flame,* ***161***, pp. 2107–2119.

[6] Yadav, R., Kushari, A., Eswaran, V., and Verma, A. K., 2014. "A detailed validation study of multi-environment eulerian probability density function transport method for modeling turbulent nonpremixed combustion". *Journal of Engineering for Gas Turbines and Power,* ***136***, pp. 081506–1–081506–11.

[7] De, A., Dongre, A., and Yadav, R., 2013. "Numerical investigation of delft-jet-in-hot-coflow (DJHC) burner using probability density funciton (PDF) transport modeling". In Proceedings of ASME Turbo Expo 2013, no. GT2013-95390.

[8] Lee, J., Jeon, S., and Kim, Y., 2015. "Multi-environment probability density function approach for turbulent CH4/H2 flames under the MILD combustion condition". *Combustion and Flame,* ***162***, pp. 1464–1476.

[9] Lee, J., and Kim, Y., 2012. "DQMOM based PDF transport modeling for turbulent lifted nitrogen-diluted hydrogen jet flame with autoignition". *International Journal of Hydrogen Energy,* ***37***, pp. 18498–18508.

[10] Akroyd, J., Smith, A. J., McGlashan, L. R., and Kraft, M., 2010. "Numerical investigation of DQMoM-IEM as a turbulent reaction closure". *Chemical Engineering Science,* ***65***(6), pp. 1915–1924.

[11] Abbrecht, P. H., and Churchill, S. W., 1960. "The thermal entrance region in fully developed turbulent flow". *American Institute of Chemical Engineers,* ***6***(2), June, pp. 268–273.

[12] Lammel, O., Stöhr, M., Kutne, P., Dem, C., Meier, W., and Aigner, M., 2012. "Experimental analysis of confined jet flames by laser measurement techniques". *Journal of Engineering for Gas Turbines and Power,* ***134***, pp. 41506–41506–9.

[13] Löwe, J., Probst, A., Knopp, T., and Kessler, R., 2016. "Low-dissipation low-dispersion second-order scheme for unstructured finite volume flow solvers". *AIAA Journal,* ***54***, pp. 2961–2971.

[14] Reichling, G., Noll, B., and Aigner, M., 2013. "Development of a projection-based method for the numerical calculation of compressible reactive flows". In Proceedings of the 51st AIAA Aerospace Sciences Meeting including the New Horizons Forum and Aerospace Exposition.

[15] Fox, R. O., 2003. *Computational Models for Turbulent Reacting Flows*. Cambridge University Press.

[16] Möbus, H., Gerlinger, P., and Brüggemann, D., 2001. "Comparison of eulerian and lagrangian monte carlo PDF methods for turbulent diffusion flames". *Combustion and Flame,* ***124***(3), pp. 519 – 534.

[17] Pope, S. B., 1976. "The probability approach to the modelling of turbulent reacting flows". *Combustion and Flame*(27), pp. 299–312.

[18] Gerlinger, P., 2005. *Numerische Verbrennungssimulation*. Springer.

[19] Villermaux, J., and Devillon, J., 1972. "Representation de la coalescence et de la predispersion des domaines de segregation dans un fluide par un modele d'interaction phenomenologique [representation of the coalescence and the predispersion of segregation domains in a fluid with a phenomenological interaction model]". In Second International Symposium on Chemical Reacting Engineering, Elsevier, pp. 1–13.

[20] Wang, L., and Fox, R. O., 2004. "Comparison of micromixing models for CFD simulation of nanoparticle formation". *American Institute of Chemical Engineers,* ***50***(9), September, pp. 2217–2232.

[21] Raman, V., Pitsch, H., and Fox, R. O., 2003. "Quadrature moment method for the simulation of turbulent reactive flows". *Annual Research Briefs*, pp. 261–275.

[22] Wilcox, D. C., 1988. "Reassessment of the scale-determining equation for advanced turbulence models". *AIAA Journal,* ***26***, pp. 1299–1310.

[23] Raithby, G., and Schneider, G., 1979. "Numerical solution

of problems in incompressible fluid flow: Treatment of the velocity pressure coupling". *Numerical Heat Transfer,* ***2***, pp. 417–440.

[24] Kazakov, A., and Frenklach, M., 1994. Reduced reaction sets based on GRI-mech 1.2. http://www.me.berkeley.edu/drm/.

[25] Yin, Y., Nau, P., Boxx, I., and Meier, W., 2015. "Characterisation of a single-nozzle floy model combustor using khz laser diagnostics". In Proceedings of the ASME Turbo Expo 2015: Turbine Technical Conference and Exposition.

[26] Gövert, S., Mira, D., Zavala-Ake, M., Kok, J., Vzquez, M., and Houzeaux, G., 2017. "Heat loss prediction of a confined premixed jet flame using a conjugate heat transfer approach". *International Journal of Heat and Mass Transfer,* ***107***, pp. 882 – 894.